CARBON 49 (2011) 1842–1848

available at www.sciencedirect.com

ScienceDirect

journal homepage: www.elsevier.com/locate/carbon

Catalyst-free formation of vertically-aligned carbon nanorods as induced by nitrogen incorporation

Richard Ritikos [a], *Saadah Abdul Rahman* [a,*], *Siti Meriam Ab. Gani* [a], *Muhamad Rasat Muhamad* [a], *Yoke Khin Yap* [b]

[a] *Low Dimensional Materials Research Centre, Department of Physics, University of Malaya, Kuala Lumpur 50603, Malaysia*
[b] *Department of Physics, Michigan Technological University, Houghton, MI 49931-1295, USA*

ARTICLE INFO

Article history:
Received 10 September 2010
Accepted 4 January 2011
Available online 9 January 2011

ABSTRACT

We found that nitrogen incorporation can induce the formation of vertically-aligned hydrogenated carbon nanorods without the use of catalysts. These nitrogen incorporated hydrogenated carbon nanorods (CN_x:H) were synthesized by radio-frequency plasma-enhanced chemical vapor deposition (PE-CVD). We have evaluated the structural and chemical evolution of these CN_x:H films as a function of the deposition duration by using high-resolution scanning electron microscopy (HRSEM), high-resolution transmission electron microscopy (HRTEM), Fourier transform infrared spectroscopy (FTIR), and Auger electron spectroscopy. Results indicate that the incorporation of nitrogen is responsible to the formation of these nanorods. The alignment of the nanorods is enhanced at longer deposition period and is correlated to the increase in nitrogen contents and isonitrile bonds [–N≡C] in the nanorods. The growth mechanism of this catalyst-free formation of nitrogen incorporated carbon nanorods is proposed.

1. Introduction

Theoretical prediction of β-C_3N_4 has stimulated tremendous efforts on the synthesis of nitrogen incorporated carbon materials [1]. While the formation of β-C_3N_4 requires nitrogen contents of 57 at.%, most reported work could achieve up to a typical of 30 at.%. Furthermore, feature-less amorphous thin films are always formed [2] with predominated sp^2-hybridized C=N bonds [3]. Although, nitrogen incorporated carbon (CN_x) films with predominant sp^3-hybridized C–N bonds can be synthesized at 600 °C by rf-plasma assisted pulsed-laser deposition (PLD), the achievable nitrogen contents are <16 at.% [4]. Despite of the on-going debates on the reality of C_3N_4 compounds, CN_x films have lead to some useful applications including electron field emission [5] and protective coatings [6]. Recent research interest on incorporating nitrogen into carbon nanomaterials have shifted into introducing donors and enhancing the electrical conductivity of carbon nanotubes (CNTs) [7,8], and graphene nanoribbons (GNRs) [9]. These nano-CN_x compounds are promising for fuel cells and nanoelectronic devices. However, the doping rates of nitrogen into CNTs and GNRs are relatively low due to the strong sp^2-hybridized C=C bonding in the graphene networks.

Here we report on the formation of new CN_x nanorods that can be synthesized at low temperatures (~100–220 °C). These nitrogen incorporated hydrogenated carbon nanorods (CN_x:H) are having high aspect ratio (diameter 20–140 nm, length up to 5 μm) with significantly high nitrogen contents (up to ~42 at.%). Furthermore, they are always grown vertically-aligned on substrates with controllable diameters and spacing without the use of catalyst. We believe that these CN_x:H

* *Corresponding author:* Fax: +603 7967 4146.
E-mail address: saadah@um.edu.my (S.A. Rahman).
0008-6223/$ - see front matter
doi:10.1016/j.carbon.2011.01.006

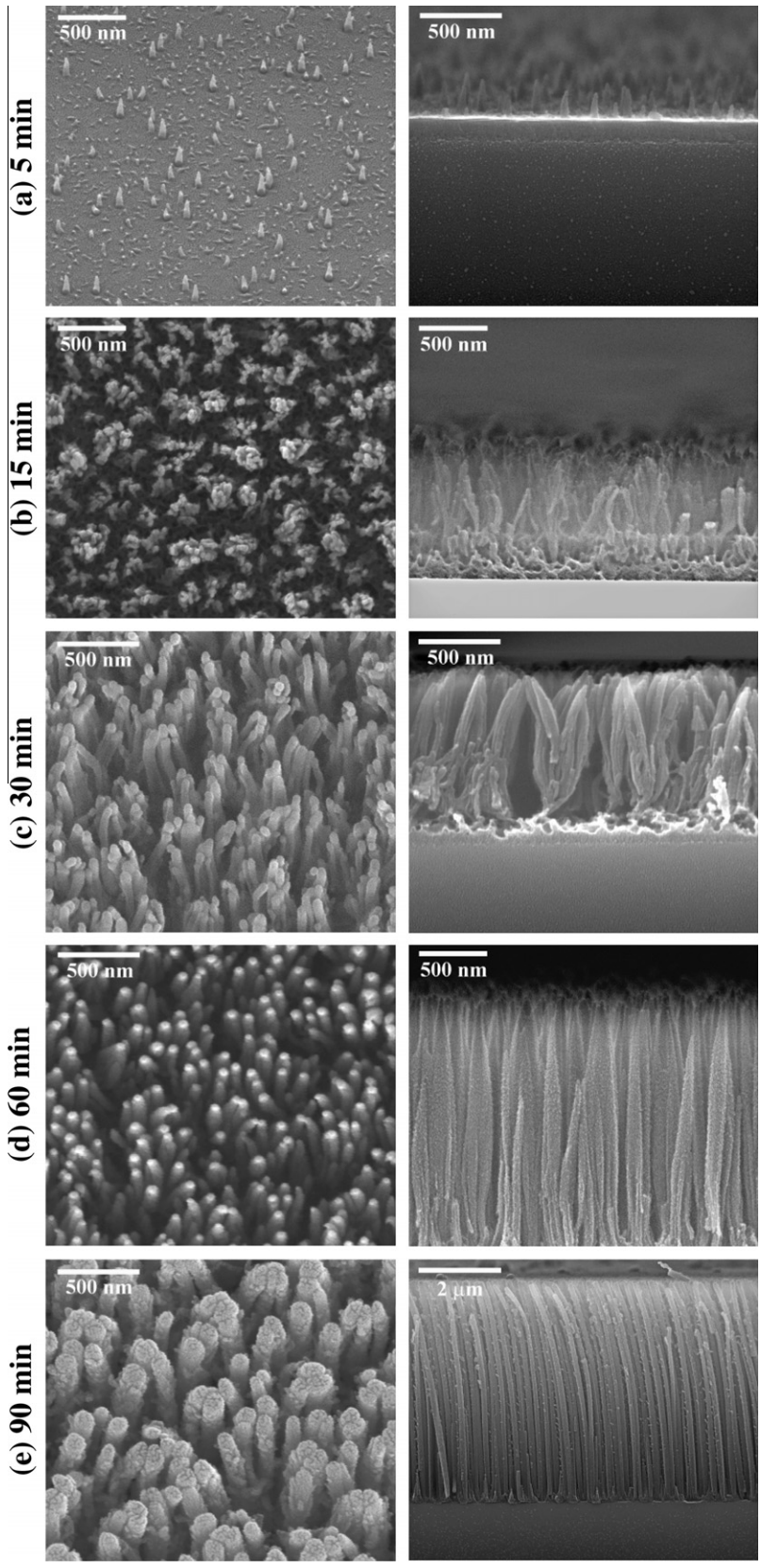

Fig. 1 – Top (left column) and cross-section (right column) views of CN_x:H nanorods obtained at varied deposition duration.

nanorods are promising for applications including large area electron field emission devices, [5] vacuum electronics, [5] miniature electron sources for X-ray generation, and electrochemical fuel cells [7].

2. Experimental

Our CN_x:H samples were grown in a custom-built rf plasma-enhanced chemical vapor deposition (PECVD) system with a parallel-plate electrode configuration. The plasma was generated using a conventional radio-frequency (13.56 MHz) power supplier connected to the top electrode. The substrates were mechanically attached on the bottom electrode with a stainless steel mask and were grounded. These electrodes are identical in area (133 cm^2) and separated by a gap of ~1 cm. Details of the system have been reported elsewhere [10]. A mixture of methane (CH_4) and nitrogen (N_2) gasses was used as the source gas. Samples were deposited on bare p-type Si (1 1 1) substrates at an rf power density of 2800 mW/cm^2 for time duration varied between 5 and 90 min. The chamber base pressure was approximately 3×10^{-5} mbar. The starting substrate temperature was set at 100 °C, though during film growth the substrate temperature increases almost linearly till it saturates after an hour of deposition at approximately 220 °C due to plasma heating. Prior to the actual deposition, the substrates were subjected to hydrogen plasma treatment for 10 min at an rf power density, a gas flow rate, and a chamber pressure of 1750 mW/cm^2, 50 sccm and 0.8 mbar, respectively.

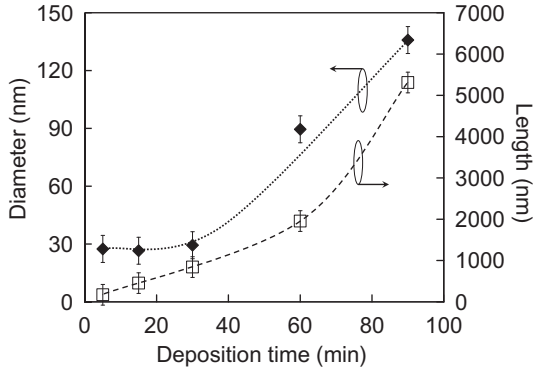

Fig. 2 – Variation of average length and diameter as a function of deposition duration.

The growth morphologies (top and cross section view) of our samples were obtained by field emission scanning electron microscopy (FESEM, FEI Quanta 200). Prior to the measurement a splashed of Au was thermally evaporated onto the films to decrease surface charging effect and improve image resolution. Auger electron spectroscopy (AES) was employed for the study of the elemental composition of these films using a Field Emission Auger Microprobe (JEOL JAMP-9500F). A series of etching-measure cycles was carried out (etching rate of 0.74 nms^{-1}) during AES measurement to minimize signal distortion and variation due to potential surface contaminants. Composition quantifications were carried out using the standard sensitivity factors of the instrument. The chemical bonding of the films was then analyzed by Fourier transform infrared (FTIR) spectroscopy. FTIR spectra were obtained in the transmission mode within the scanning range of

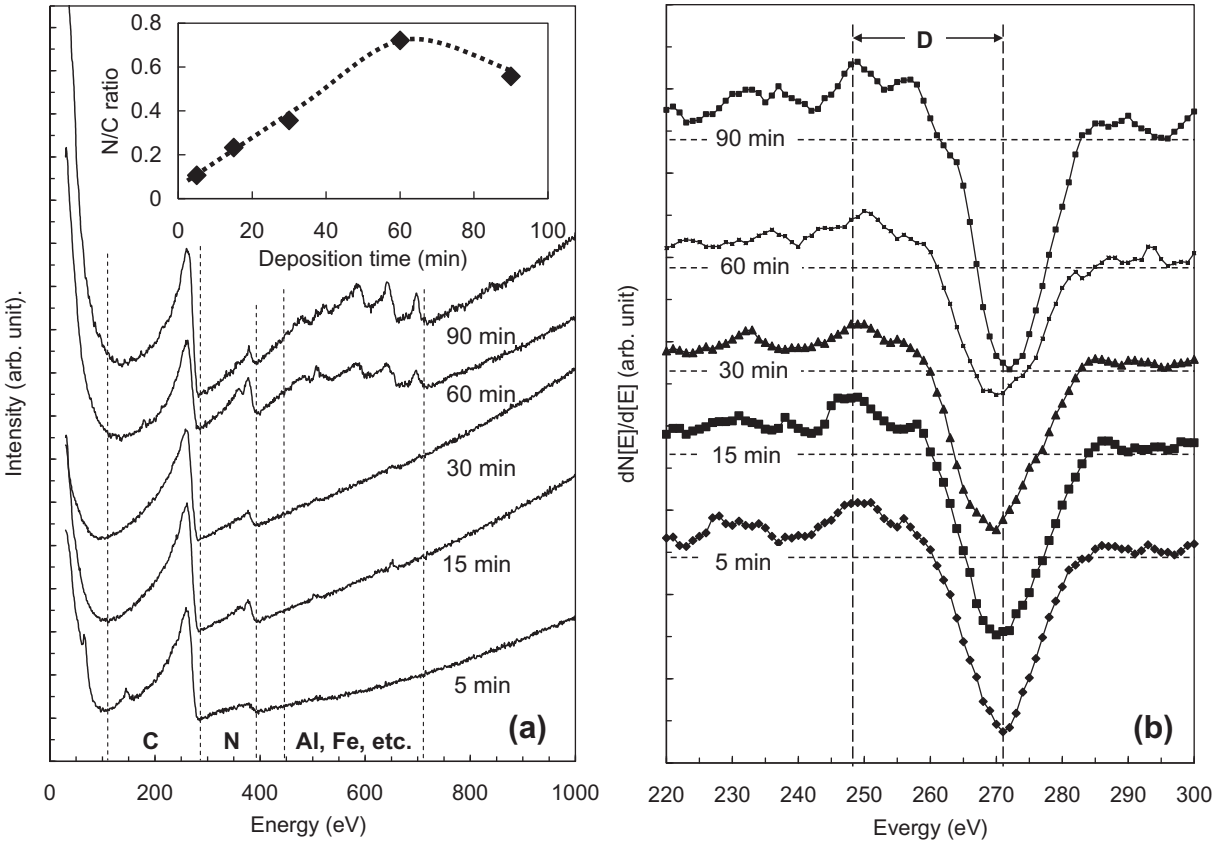

Fig. 3 – Variation of AES spectra for (a) wide spectra scan, and (b) first derivatives CKVV spectra, as a function of deposition time. The inset in (a) is the variation of N/C ratio as a function of deposition duration.

1000–4000 cm^{-1} using a Perkin-Elmer System 2000 FTIR spectrometer. High-resolution transmission electron microscopy (HRTEM) was used to characterize the nanorods using a JEOL JEM-2100F system operated at 200 kV of acceleration voltage. This system was equipped with an energy dispersive X-ray (EDX) analyzer.

3. Results and discussion

The variation in growth morphology obtained from FESEM is shown in Fig. 1 as a function of the deposition duration, T_d. As shown, the growth of the CN_x:H nanorods begins with the formation of short nanorods on the bare Si substrates. These nanorods grew irregularly both in distribution and length. The density of the nanorods and the vertical alignment were enhanced with the increase of T_d. Fig. 2 summarizes the variation in the length and diameter of the nanorods as a function of T_d. As shown, the lengths and the diameters of the CN_x:H nanorods increase progressively with T_d. The lengths are measured from the cross section images in Fig. 1, between the tips of the nanorods and the substrate surface, while the diameters are estimated at the center of the nanorods. Fig. 1a–c indicates that within the initial 30 min, the nanorods are not well oriented and slightly bended. As shown in Fig. 2, the diameter of the structures increases significantly after T_d ~30 min. We think that the increase in diameter will create constriction between neighboring nanorods and forced them to grow more vertically aligned thereafter as shown in Fig 1d and e. The adhesion between the nanorods and Si substrates is relatively stronger than what we typically observed for CNTs grown on Si substrates. This was judged by scratching of the coatings by tweezers.

AES measurements were carried out in a wide scan spectrum to investigate the composition of the films. The spectra of the AES measurement and the corresponding first derivation of the spectra are shown in Fig. 3. The expected peaks corresponding to those of carbon and nitrogen in the energy range of 170–300 eV and 330–410 eV, respectively are apparent for all the thin film samples. However, at longer T_d the spectra reveal a certain amount of contaminants which originates from the sputtering of the components in the deposition chamber itself. Since the contaminants (mostly metal such as Fe and Al) were not measurable during 2/3 of the full deposition duration (up to T_d of 30 min), we think that these metals did not act as the catalyst for the formation of these CN_x:H nanorods. As we will discuss later, we proved that nitrogen incorporation is the major factor for the formation of the nanorods. The nitrogen to carbon (N/C) ratios for all samples are summarized in the inset in Fig. 3a. The N/C ratio increases linearly with T_d and begins to saturate at $T_d > 60$ min. The maximum N/C ratio at $T_d = 60$ min is significantly high (~0.73) and corresponds to a nitrogen concentration of 42 at.%.

The first derivative spectra were used to investigate the bonding properties of the structures in terms of the sp^2 and sp^3 concentration in the films. As shown in Fig. 3b, the difference in the value of the most positive and most negative excursions of the carbon KLL peak which is usually referred to as the D value [11], changes according to the sp^2/sp^3 ratio in the sample. This is most commonly done using the spectra of graphite (pure sp^2) and diamond (pure sp^3) samples as comparison. The D value of graphite is taken as approximately 21, while that of diamond is taken as 13–14 [12]. According to Turgeon and Paynter [11], the D value varies linearly with the sp^2/sp^3 ratio and thus the values obtained for graphite and diamond could be used for calibration standards. From the CKVV spectra obtained for the nanorods, the values calculated were approximately 21–22 and do not vary with T_d. This indicates that the sp^2/sp^3 ratios of the films are similar and are not affected by the deposition duration. Furthermore the values obtained are similar to that of graphite and indicates that the sp^2–C bonds in the films outweigh any presence of sp^3 in the film. On the other hand, an overlapping peak at approximately 277 eV, which is particularly noticeable for $T_d = 60$ min, indicates the sp^2 bonded carbon atoms are present in a disordered carbon matrix [12].

FTIR absorption spectra for our CN_x:H nanorods are shown in Fig. 4 and are similar to that of polymeric hydrogenated amorphous carbon nitride films reported elsewhere [13]. These spectra show the presence of the N–H, C=C, and/or C=N stretching (1300–1800 cm^{-1}), C–H_n groups (2800–3000 cm^{-1}), C≡N groups (2000–2200 cm^{-1}) and N–H and/or O–H bonds (3000–3700 cm^{-1}) [14,15] in our CN_x:H nanorods. The O–H bonds in a-C:H may be due to post-contamination of hydroxyl absorbed in the pores of the material [16]. Though

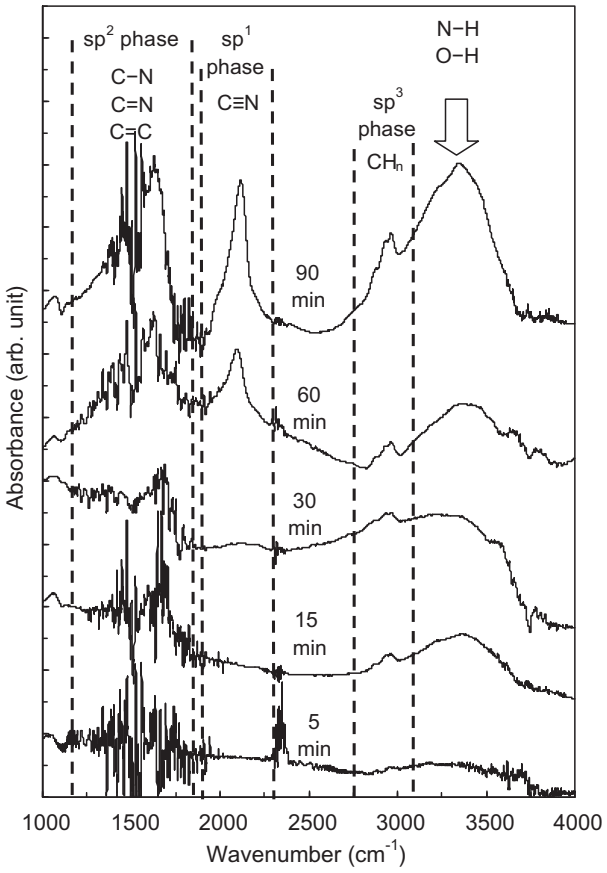

Fig. 4 – FTIR absorbance spectra as a function of deposition duration.

weak, the presence of sp^3 bonds in the films contributed by the C–H_n groups could not be ignored. Consistent with the AES results, the preference of sp^2 bonds in the samples is supported by the stronger and more prominent band in the region of 1000–1800 cm^{-1} contributed by the N–H, C=C, and/or C=N stretching bands. In addition, there is an obvious increase in C≡N bonds after the 30 min deposition duration.

To further interpret the FTIR spectra of our CN_x:H nanorods, two additional thin film samples were prepared for comparison. The first one is a hydrogenated carbon film (a-C:H) deposited under similar conditions as our CN_x:H nanorods except that only pure methane was used without nitrogen gas. This deposition gives a smooth hydrogenated carbon film without any evidence of nanorods. This means, nitrogen incorporation is responsible to the formation of CN_x:H nanorods. The second sample is a polymeric a-CN_x:H film similar to those reported elsewhere [13]. Fig. 5 shows the variation of the FTIR spectra and the corresponding FESEM images for the (1) CN_x:H nanorods reported here, (2) smooth a-C:H thin film and (3) polymeric a-CN_x:H film previously reported [13].

By comparing FTIR of these three types of samples, we conclude that the type of incorporated carbon–nitrogen bonds is crucial for the formation of our CN_x:H nanorods. As shown in Fig. 5, the obvious difference between these samples is that the CN_x:H nanorods have a significant strong peak in the region of the sp^1 bonded C≡N (~2115 cm^{-1}). This prominent peak is not observed in the smooth a-C:H thin film and the polymeric a-CN_x:H film and thus is interpreted as one of the main criteria for the formation of the CN_x:H nanorods. This peak has been assigned as isolated and/or fused aromatic rings bonded to isonitrile (–N≡C) [15,17]. This bond is non-terminating and would promote the formation of long range ordering structures. This functional group is connected to the graphitic ring through N atom rather than C. This means, the nitrogen atom will have a positive charge while C will be negatively charged (i.e., $-N^+\equiv C^-$). Thus the resulting carbon network would have a partial charge imposed on it by the presence of this bond. From Fig. 4 the absorbance intensity of this peak increases with the increase in T_d and implies that the contents of the charged [$-N^+\equiv C^-$] bonds are increased with T_d. Furthermore, since the rf plasma is generating electric field in the direction perpendicular to the substrate surface, we believe that this electric field will induce aligned deposition of these polarized [$-N^+\equiv C^-$] bonds and contribute to the formation of vertically-aligned nitrogen incorporated carbon nanorods reported here.

Fig 6 shows the HRTEM images of the CN_x:H nanorods deposited for 90 min. Fig. 6a shows the upper tip of the vertically aligned nanorods. These nanorods appear to have randomly distributed nanocrystallites with cluster size ranging from approximately 2–20 nm in diameter. In Fig. 6b both the selected area electron diffraction (SAED) pattern and the

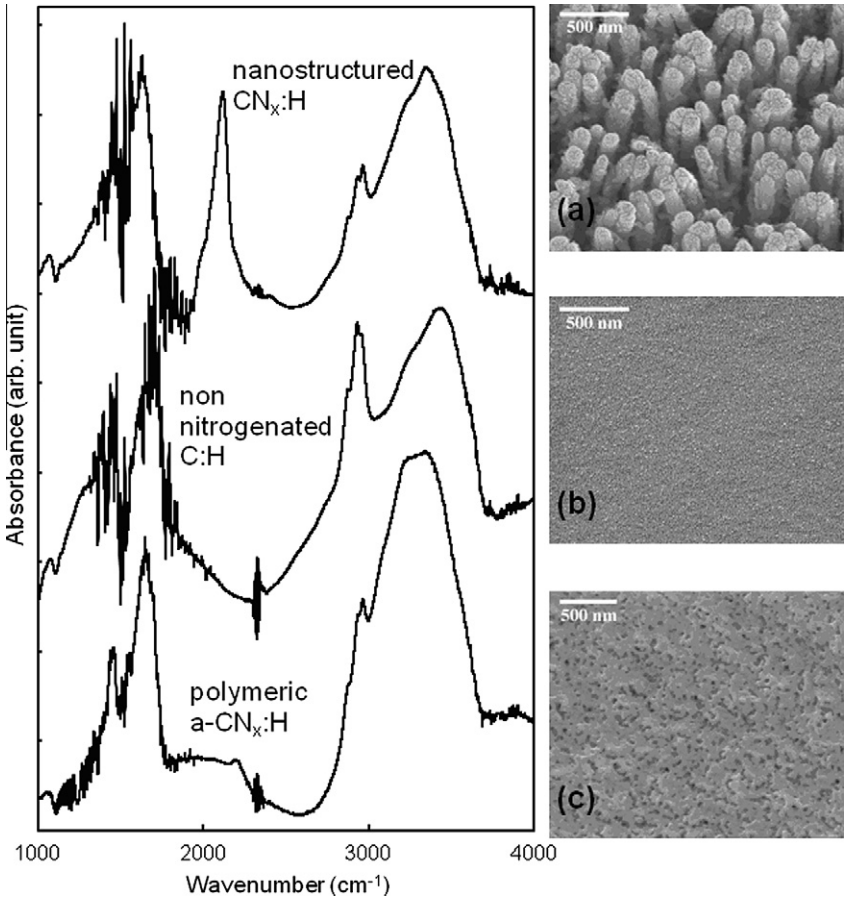

Fig. 5 – Comparison of FTIR spectra for (a) CN_x:H nanorods reported here, (b) smooth and non-nitrogenated a-C:H film and (c) polymeric a-CN_x:H film with the corresponding FESEM images.

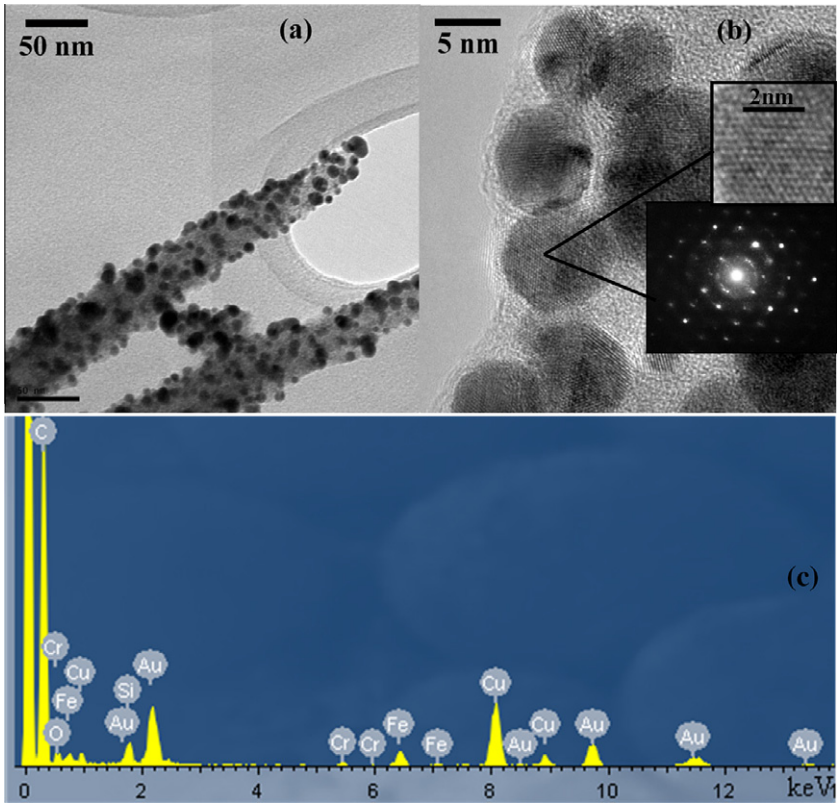

Fig. 6 – (a and b) TEM images at varied magnification for the upper tip of the nanorods formed for the deposition time of 60 min. SAED patterns (inset) and (c) EDX spectrum on the nanocrystals are shown together.

atomic resolution image (insets) show that these nanocrystals have 6-fold symmetry hexagonal structure. The ratio of inter-plane distances between d_{100} and d_{110} can be calculated as ~1.7, identical to that of graphite (d_{100}/d_{110} = 1.732). We further conducted high-resolution EDX analysis on these nanocrystals. As shown in Fig. 6c, these crystallites consist of carbon, with no detectable content of nitrogen. Au is detected as the sample was coated with Au film prior to SEM imaging. Other trace signals are from the TEM grid and contaminants originated from the deposition chamber. Based on these results, we conclude that these clusters are graphite nanocrystals. We believe that nitrogen is integrated in the surrounding amorphous matrix.

4. Growth mechanism

Based on what have been discussed so far, we propose a growth mechanism for our CN_x:H nanorods. The illustrations of the proposed mechanism are shown in Fig. 7. We think that the directional electric field generated by the rf plasma is important for the formation of our CN_x:H nanorods. This electric field initiated directional flux of ionic growth species of carbon and nitrogen. Apparently, carbon nitrate phase is energetically less stable than the graphite phase [4]. Thus, crystallized phase of nano-graphite is formed while the carbon nitrate phase remained as amorphous as shown in Fig. 7a. Due to the close proximity of the electrodes, intensive

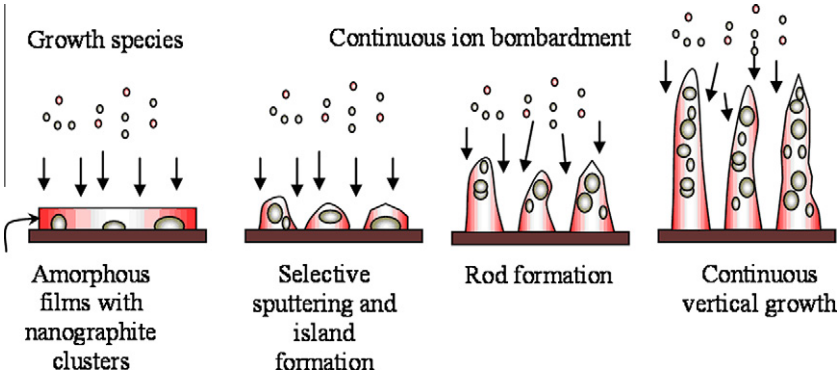

Fig. 7 – The illustrations of the proposed growth mechanism for the nanorods.

ion bombardment on the growing surface is expected. Apparently, the crystallized graphite phase has higher resistance to plasma etching than the amorphous carbon nitrate phase. This has lead to higher etching rate of the amorphous component and left behind the more stable islands that have more graphite inclusion. This is why lower nitrogen contents were detected at short deposition duration. The amorphous phase functions as the matrix that holds the graphite nanoclusters together and form scattered islands as shown in Fig. 1a. As the grow process continue, these islands will grow in size [Fig. 7c and d] and stabilize more amorphous carbon–nitrogen phase as thus increase the overall nitrogen contents of our samples with the increase of deposition duration. Owing to the directional flux of the grow species, and the sub-implantation process in the direction normal to the substrate surface, the columnar growth mode will dominate the lateral diffusion. Thus, vertically-aligned nanorods are formed on the initial islands. In addition, the isonitrile bond [$-N^{+}\equiv C^{-}$] in the amorphous matrix creates a charge polarity that promotes the columnar growth mode as they tend to align along the direction of the electric field. Such an electric field driven formation of aligned nanorods is as interesting and as novel as a recently reported leaf-like carbon nitride nanorods [18].

5. Conclusion

The effect of deposition duration, T_d on the formation of CN_x:H nanorods has been studied in terms of the structural and chemical bonding characteristics. Our results provide new insights on the synthesis of catalyst-free CN_x:H nanorods at low temperatures. Both the vertical alignment and nitrogen contents of these CN_x:H nanorods were increased with the deposition duration up to T_d = 60 min. The additional nitrogen in the nanostructures is bonded in the isonitrile configuration which incites a charging polarity in the nanostructured strands. The incorporated nitrogen is presented in the amorphous phase which surrounds, encapsulates and holds the nanographite crystallites together.

Acknowledgments

This work was supported by the Ministry of Science, Technology and Innovation (MOSTI), Malaysia under the Fundamental Research Grant Scheme FP016/2008C, FP052/2010B and the University of Malaya (Grants FS290/2008C and RG064/09AFR). Due acknowledgment also goes to the University of Malaya staff training scheme (SLAI). The authors thank Dr. Norlida Kamarulzaman of the University Technologi MARA, Malaysia for the HRTEM micrographs. Yoke Khin Yap acknowledge supports from the Brain Gain Malaysia program (MOSTI, Malaysia), and the US National Science Foundation CAREER award (Award No. 0447555).

REFERENCES

[1] Liu AY, Cohen ML. Prediction of new low compressibility solids. Science 1989;245:841–2.
[2] Robertson J. Diamond-like amorphous carbon. Mater Sci Eng R 2002;37:129–281.
[3] Hu JT, Yang PD, Lieber CM. Nitrogen-driven sp^3 to sp^2 transformation in carbon nitride materials. Phys Rev 1998;B57:R3185–8.
[4] Yap YK, Kida S, Aoyama T, Mori Y, Sasaki T. Influence of negative dc bias voltage on structural transformation of carbon nitride at 600 °C. Appl Phys Lett 1998;73:915–7.
[5] Yap YK, Kida S, Aoyama T, Mori Y, Sasaki T. Effect of carbon nitride bonding structure on electron field emission. Diamond Relat Mater 2000;9:1228–32.
[6] Cutiongco EC, Li D, Chung YW, Bhatia CS. Tribological behavior of amorphous carbon nitride overcoats for magnetic thin-film rigid disks. J Tribol 1996;118:543–5.
[7] Gong K, Du F, Xia Z, Durstock M, Dai L. Nitrogen-doped carbon nanotube arrays with high electrocatalytic activity for oxygen reduction. Science 2009;323:760–4.
[8] Yap YK. B-C-N Nanotubes and Related Nanostructures. Lecture Notes in Nanoscale Science and Technology. Springer; 2009 [chapters 1, 3, 7, 8 therein].
[9] Wang X, Li X, Zhang L, Yoon Y, Weber PK, Wang H, et al. N-doping of graphene through electrothermal reactions with ammonia. Science 2009;324:768–71.
[10] Ritikos R, Goh BT, Sharif KAM, Muhamad MR, Rahman SA. Highly reflective nc-Si:H/a-CN_x:H multilayer films prepared by rf PECVD technique. Thin Solid Films 2009;517:5092–5.
[11] Turgeon S, Paynter RW. On the determination of carbon sp^2/sp^3 ratios in polystyrene polyethylene copolymers by photoelectron spectroscopy. Thin Solid Films 2001;394:44–8.
[12] Popov C, Plass MF, Zambov L, Bulir J, Delplancke-Ogletree MP, Kulisch W. Physical properties of carbon nitride films synthesized using atomic transport reactions. Surf Coat Tech 2000;125:278–83.
[13] Ritikos R, Chow CS, Gani SM, Muhamad MR, Rahman SA. Effect of annealing on the optical and chemical bonding properties of hydrogenated amorphous carbon and hydrogenated amorphous carbon nitride thin films. Jpn J Appl Phys 2009; 48:101301(−1)–(−4).
[14] Motta EF, Pereyra I. Amorphous hydrogenated carbon-nitride films prepared by RF-PECVD in methane–nitrogen atmospheres. J Non-Cryst Solids 2004;338–340:525–9.
[15] Mutsukura N, Akita K. Photoluminescence and infra-red absorption of hydrogenated amorphous CN_x films. Diamond Relat Mater 2000;9:761–4.
[16] Fanchini G, Mandracci TP, Tagliaferro A, Rodil SE, Vomiero A, Della Mea G. Growth and characterization of polymeric amorphous carbon and carbon nitride films from propane. Diamond Relat Mater 2005;14:928–33.
[17] Mutsukura N, Akita K. Deposition of hydrogenated amorphous CN_x film in CH_4/N_2 rf discharge. Diamond Relat Mater 1999;8:1720–3.
[18] Li Y, May PW, Yin L, Brown R, Scott TB. Direct growth of highly organized crystalline carbon nitride for liquid-phase pulsed laser ablation. Chem Mat 2006;18:5058–64.